AGU PUBLICATIONS

Tectonics

RESEARCH ARTICLE
10.1002/2017TC004647

Key Points:
- Quantification of tectonic and climatic controls on sedimentation in asymmetric extensional basins
- New insights into distribution of lithologies, sedimentary facies, and unconformities in half-grabens
- Verifying the new insights in the Pannonian Basin tectono-sedimentary evolution

Supporting Information:
- Supporting Information S1

Correspondence to:
A. Balázs,
a.balazs@uu.nl

Citation:
Balázs, A., Granjeon, D., Matenco, L., Sztanó, O., & Cloetingh, S. (2017). Tectonic and climatic controls on asymmetric half-graben sedimentation: Inferences from 3-D numerical modeling. *Tectonics*, *36*, 2123–2141. https://doi.org/10.1002/2017TC004647

Received 2 MAY 2017
Accepted 11 SEP 2017
Accepted article online 18 SEP 2017
Published online 23 OCT 2017

Tectonic and Climatic Controls on Asymmetric Half-Graben Sedimentation: Inferences From 3-D Numerical Modeling

Attila Balázs[1], Didier Granjeon[2], Liviu Matenco[1], Orsolya Sztanó[3], and Sierd Cloetingh[1]

[1]Netherlands Research Center for Integrated Solid Earth Science, Faculty of Geosciences, Utrecht University, Utrecht, Netherlands, [2]Department of Geology-Geophysics-Geochemistry, IFP Energies Nouvelles, Rueil-Malmaison, France, [3]Department of Physical and Applied Geology, Eötvös Loránd University, Budapest, Hungary

Abstract The tectono-sedimentary evolution of asymmetric extensional systems driven by the activity of major normal faults or detachments associated with footwall exhumation is often characterized by a sequence of slower, faster, and ultimately again slower subsidence rates in the center of hanging wall half-grabens during their synkinematic and postkinematic evolution. We have studied this specific evolution by the means of 3-D stratigraphic numerical modeling that accounts for the variability of the sediment and water flux combined with climatic and sea level variations, and sediment compaction. The model setup is constrained by observations from the Pannonian back-arc basin of central Europe. Our modeling predicts the formation of low-order tectonic and higher-order sea level and climate-driven transgressive-regressive sedimentary cycles. Furthermore, we model and analyze the autocyclic nature of the depositional systems. Retrograding-prograding cycles are visible on the proximal flank of the half-grabens by their different spatial and temporal expressions, while depocenters record large water depth variations linked to the specific and episodic activity of normal faults and their migration with time. The application to a system of multiple half-grabens in the Pannonian Basin, which are activated in different locations, at different times and with different kinematics, demonstrates a complex interplay between direct sediment sourcing and the sediments' ability to bypass trapping subbasins and paleo-reliefs created by eroded footwalls.

Plain Language Summary The formation and evolution of sedimentary basins is of prime interest as they record different Earth processes. The understanding of rifting mechanics and associated evolution of extensional sedimentary basins is also important for the assessment of their potential for georesources including freshwater. The spatial and temporal variabilities of vertical movements in asymmetric extensional systems control landscape evolution coupled to sedimentary and climatic processes. This paper aims to quantify the effect of tectonics and climatic variations on the overall architecture of such basins. Our numerical modeling demonstrates the low-order tectonic and higher-order sea level and climate-driven influence on the sedimentary transport routes and overall architecture. The application of our model in the Pannonian Basin of central Europe shows how tectonic inheritance control sedimentary transport routes.

1. Introduction

The evolution of extensional sedimentary basins is driven by a complex interplay between the mechanics of the system combined with external and internal forcing factors, such as tectonics, climate, source areas, surface processes, geometry of depocenters, and autocyclic sedimentary processes (e.g., Cloetingh et al., 2013). Current models of synkinematic and postkinematic depositional response to extension are not directly applicable in places where series of genetically linked half-grabens, bounded by one major normal fault or detachment, control the coeval sedimentation (Figure 1) (Ellis, Densmore, & Anderson, 1999; Prosser, 1993; Tirel, Brun, & Burov, 2008; Wernicke, 1992). The spatial and temporal variabilities of vertical movements in such asymmetric extensional systems are important also for understanding landscape evolution, changes in the location of depocenters, and stratigraphic architecture (e.g., Andrić et al., 2017; Contreras, Scholz, & King, 1997; Gupta et al., 1998; Ter Voorde et al., 1997). Observed differential vertical movements are primarily controlled by patterns of crustal and lithospheric thinning coupled with the evolution of the underlying asthenosphere, strongly influenced by rheological composition, amounts of extension, localization, rate, and variability of strain (e.g., Balázs et al., 2017, and references therein). Furthermore, the tectono-sedimentary evolution of extensional basins is intrinsically coupled to surface processes in terms of erosion and

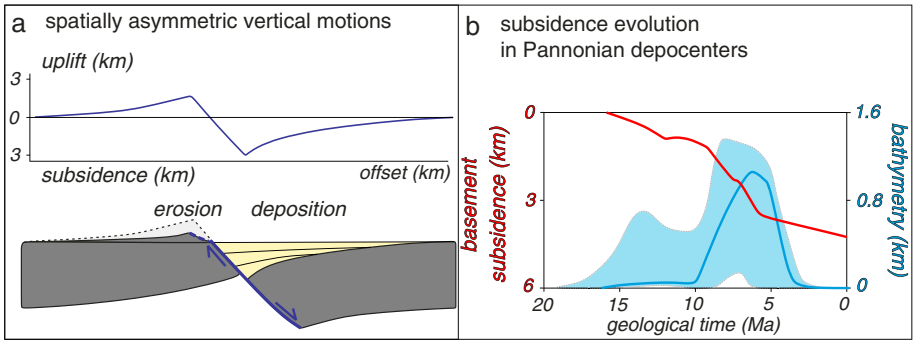

Figure 1. Simplified model of half-graben evolution controlled by a large offset listric normal fault with a dip angle of 40°, average hanging wall subsidence of 3–4 km, and flexural uplift and erosion of the footwall. (a) Asymmetric hanging wall subsidence is associated with uplift and exhumation of its footwall. Differential vertical movements are enhanced and localized by footwall erosion and hanging wall sedimentation. (b) Temporal evolution of depocenter subsidence (red curve) and paleo-water depth trend (blue area) generalized from half-grabens from the Pannonian Basin, derived from this study and previously published data (Balázs et al., 2016; Báldi, Benkovics, & Sztanó, 2002; Horváth, Szalay, & Royden, 1988). The continuous blue curve shows the paleo-water depth evolution of the Szeged subbasin.

sedimentation, which are controlled also by climatic variations (e.g., Bialas & Buck, 2009; Burov & Poliakov, 2003; Cloetingh & Haq, 2015; Maniatis et al., 2009; Olive, Behn, & Malatesta, 2014). Internal surface processes, such as footwall erosion and hanging wall sedimentation, enhance and localize vertical movements (Ellis et al., 1999; Leeder, Harris, & Kirkby, 1998). All these processes create a large spatial and temporal variability of extensional geometries (e.g., van Wijk & Cloetingh, 2002) that are often associated with a sequence of slower, faster, and ultimately again slower subsidence rates in the center of half-grabens during the synkinematic and postkinematic evolution (Figure 1). This subsidence evolution differs significantly from the rapid synrift followed by decreasing postrift patterns of classical extensional models (e.g., Balázs et al., 2017; Baur, Sutherland, & Stern, 2014). In back-arc settings, rapid basin subsidence episodes are associated with variable extensional pulses created by slab roll-back and further mantle dynamics (Faccenna et al., 2014). In such overall settings, the sedimentary response to extension is not sufficiently understood.

The sedimentary architecture of half-grabens is the result of a balance between the rate of creating accommodation space and the external or internal sediment supply, combined with sedimentary transport processes within the basin (e.g., Postma et al., 2008; Schlager, 1993). The sedimentary infill of these extensional basins is controlled by tectonic subsidence pulses. These pulses create tectonic system tracts, which are genetically linked depositional systems controlled dominantly by tectonics, bounded by key stratigraphic surfaces (cf. Prosser, 1993). The geometry and composition of the basin fill are also influenced by higher-frequency autocyclic processes, such as channel incision, filling and avulsion, lateral migration of the delta system, and lobe switching, which create onlap surfaces even without changing the overall subsidence or discharge rates (van Dijk, Postma, & Kleinhans, 2009). Different depositional concepts driven by the interpretation of geological and geophysical data (Figure 2) can be quantitatively tested by recent advances in 3-D numerical modeling techniques. These 3-D models provide the possibility to simulate sedimentation and related lithologies at higher resolution, accounting for the influence of tectonic and climatic forcings, such as variable subsidence and uplift rates, eustatic water-level variations, sediment and water discharge, and transport processes (e.g., Clevis, De Boer, & Nijman, 2004; Granjeon, 2014).

A probably ideal case for conceptual understanding of sedimentation in asymmetric extensional systems is the Pannonian back-arc basin of central Europe, where the extended database required to model numerically these concepts and to define generic links between extension and sedimentation is already available (Figure 2). Here the Great Hungarian Plain recorded the temporal and spatial formation and migration of half-grabens during the Miocene back-arc extension related to the Carpathian slab roll-back (e.g., Balázs et al., 2016; Horváth et al., 2015; Matenco et al., 2016), often associated with contrasting patterns of decreasing and subsequently increasing synrift subsidence (Figure 2c). These Miocene subbasins are flanked by large-offset low-angle normal faults or detachments and are filled by up to 3.5 km of synkinematic sediments, deeply buried beneath the subsequent late Miocene-Quaternary postrift deposits (Figure 2). The overall total

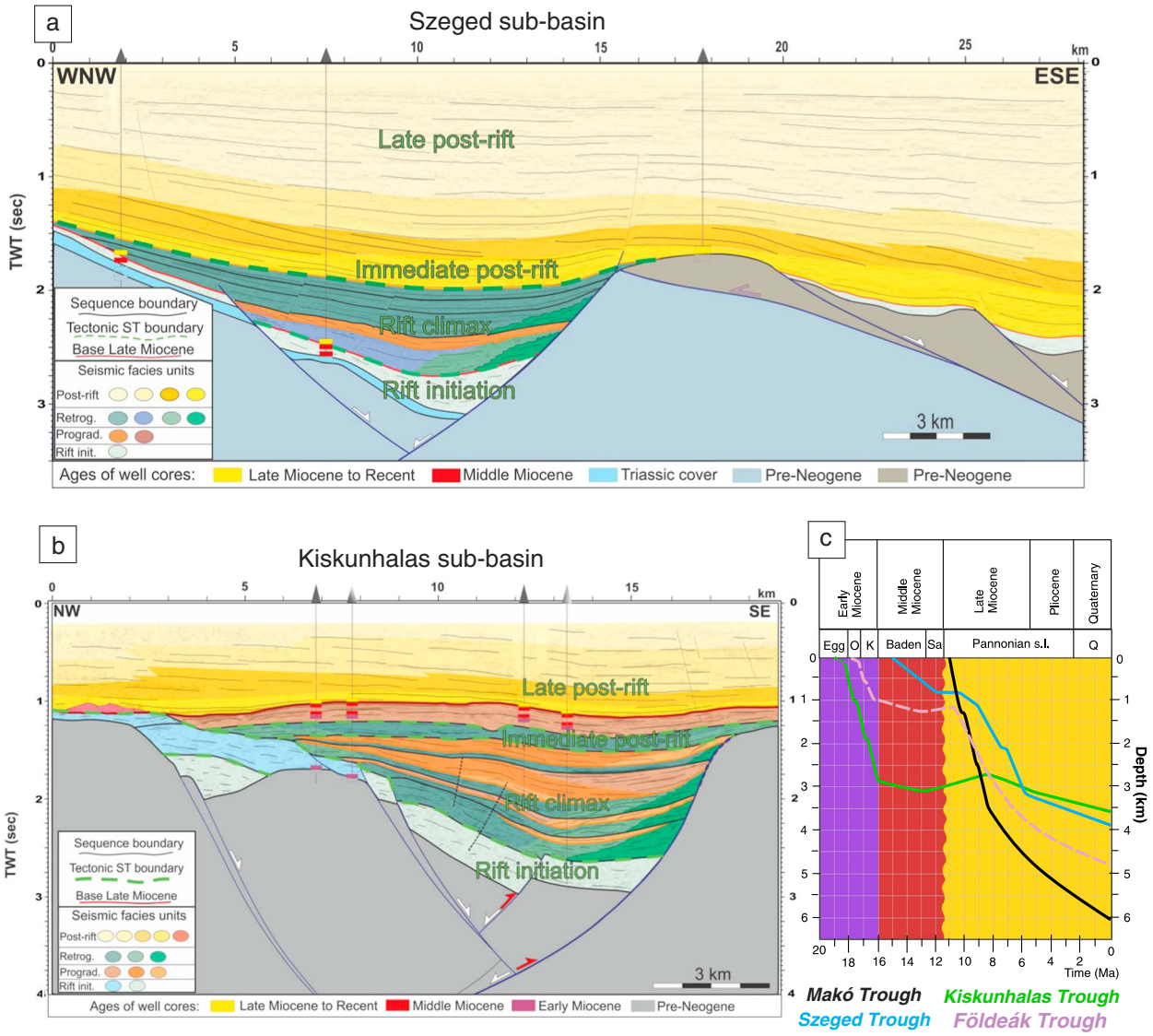

Figure 2. Tectono-sedimentary evolution of the Pannonian Basin based on interpretation of reflection seismic profiles calibrated by high-resolution well data from the (a) Szeged and (b) Kiskunhalas half-grabens (modified from Balázs et al., 2016) illustrating key features of the conceptual model. In the Szeged subbasin, rift initiation sediments are overlain by a retrograding-prograding cycle followed by a general retrogradation during late synrift times. In the Kiskunhalas subbasin, synrift retrograding-prograding cycles are grouped into lower order rifting phases (rift climax). The white arrows indicate Miocene kinematics of faults; the red arrows show the latest middle–early late Miocene inversion. Locations are displayed in Figure 10. (c) Basement subsidence curves calculated from seismic and well data in the main subbasins modeled in the Pannonian Basin showing migration of extension and episodes of fast subsidence in time (adopting Paratethys endemic timescale stages Egg, Eggenburgian; O, Ottnagian; K, Karpatian; Sa, Sarmatian).

sediment thickness reaches ~7 km in the main depocenters (e.g., Horváth et al., 2015; Tari et al., 1999, and references therein).

In this study, we investigate the link between tectonics, climate, and sedimentation during the formation and evolution of half-grabens associated with footwall exhumation by the means of 3-D numerical stratigraphic forward modeling. We analyze the evolution of one generic half-graben by defining a reference model and performing a parametric study. Subsequently, the evolution of a system of half-grabens is modeled, with a structure and sediment flux parameters inspired by the Miocene evolution of the Pannonian Basin. These parameters have general average values observed in natural examples elsewhere. Therefore, this integrated approach yields a generic quantitative understanding of the link between tectonics and sedimentation in asymmetric extensional systems, including lithological distributions and formation of unconformities, and their connections with the main forcing factors.

2. Methodology

Numerical forward modeling is particularly well suited to understand facies distribution during the evolution of sedimentary basins. Two classes of stratigraphic and geomorphologic forward models are commonly available. Models of the first class solve small-scale physical laws, such as the Navier-Stokes equation to simulate local and complex interactions between basin deformation, water flow, and sediment transport at high spatial and temporal resolutions (e.g., de Leeuw, Eggenhuisen, & Cartigny, 2016; Griffiths et al., 2001). Models of the second class follow more regional approaches and usually solve a diffusion equation that enables the modeling of sedimentary systems at larger spatial and temporal scales, and the integrated analysis of transport processes. Such diffusion laws in various forms are commonly used to represent the large-scale, spatially averaged sediment transport (e.g., Carson & Kirkby, 1972; Culling, 1960; Granjeon, 1997; Postma et al., 2008).

2.1. Modeling Approach

All numerical experiments were performed with the 3-D deterministic forward numerical modeling software DionisosFlow (e.g., Granjeon, 2014). The physical equations are solved using a finite-volume implicit numerical scheme (Gervais & Masson, 2004). This model accounts for spatial and temporal variable subsidence and erosion rates, a sediment influx composed of different sediment classes, compaction, eustasy, water discharge, sediment supply, and transport processes (see the supporting information). The overall conceptual modeling approach is also described in details elsewhere (e.g., Csató et al., 2013; Granjeon & Joseph, 1999).

The numerical modeling approach combines empirical water and gravity-driven diffusion equations, which include a slow slope-driven creeping law and a faster nonlinear water-driven and slope-driven diffusion equation. This approach leads to the following sediment transport equation (Granjeon, 2014):

$$Q_{s_i} = -K_{s_i} S - K_{w_i} \hat{Q}_w^m S^n, \text{ where } \hat{Q}_w = Q_w / Q_{w_0} \quad (1)$$

where Q_{s_i} is the flux of the ith sediment class ($m^2\ s^{-1}$), K_{s_i} is a creeping diffusion coefficient, S is the local slope gradient, K_{w_i} is a water-driven diffusion coefficient, $\hat{Q}_w$ is a local normalized water discharge with $Q_{w_0} = 1\ m^3\ s^{-1}$, m and n are power coefficient constants between 1 and 2 (Tucker & Slingerland, 1994), and i is the index of the grain size fraction.

This transport equation reflects the general depositional process during erosion, transport, and deposition at basin scale (Burgess et al., 2006). In classical landscape evolution numerical experiments, fluvial water flow is modeled using a single-direction routing method, where water flows toward the steepest slope (e.g., Tucker & Slingerland, 1994). The approach of DionisosFlow is different by simulating the behavior of the entire sedimentary basin system at a larger scale. This regional approach uses a multidirection method (Granjeon, 2014), where water is routed to all local lower neighbors of a given cell following slope ratios, which handles better diverging flow pattern (Tucker & Hancock, 2010) and is well adapted to simulate overland sheet flow as well as braided systems (Coulthard, 2001; Murray & Paola, 1994).

In our modeling we use three grain-size fractions: basement-derived pebble, sand, and mud fraction. A wide range of diffusivity coefficient values (K_s and K_w in equation (1)) were used in previous numerical studies. These coefficients reflect the ratio of sediment discharge and basin slope, more fine-grained sediments showing higher values than coarse-grained ones. We used average diffusion coefficients for coarse- and fine-grained fractions in our modeling scenarios that are similar to previous DionisosFlow models (e.g., Gvirtzman, Csató, & Granjeon, 2014), i.e., 80 and 160 km^2/kyr and 0.08 and 0.8 km^2/kyr for sand and mud water-driven diffusion coefficients in continental and marine environments, respectively. Each voxel is made up by a mixture of the above mentioned lithologies that are visualized by the proportion of sand or basement-derived fractions, in other words, how coarse-grained is a modeled volume. The sedimentation and erosion rate at each time step is computed from the local sediment flux assuming mass conservation in the basin. This means that sedimentation occurs in the basin if the transport capacity decreases, in other words, when the divergence of the flux is negative. On the contrary, erosion occurs if the transport capacity increases. The erosion rate predicted by the transport equation cannot exceed a maximum mechanical incision rate. Similar to previous studies, the maximum erosion rate induced by water flow and sediment transport is limited to a value of 0.3 mm/yr, which is a reasonable assumption for Miocene extensional basins, for instance, in the Pannonian Basin (e.g., Karátson et al., 2006). Compaction of sediments is computed following

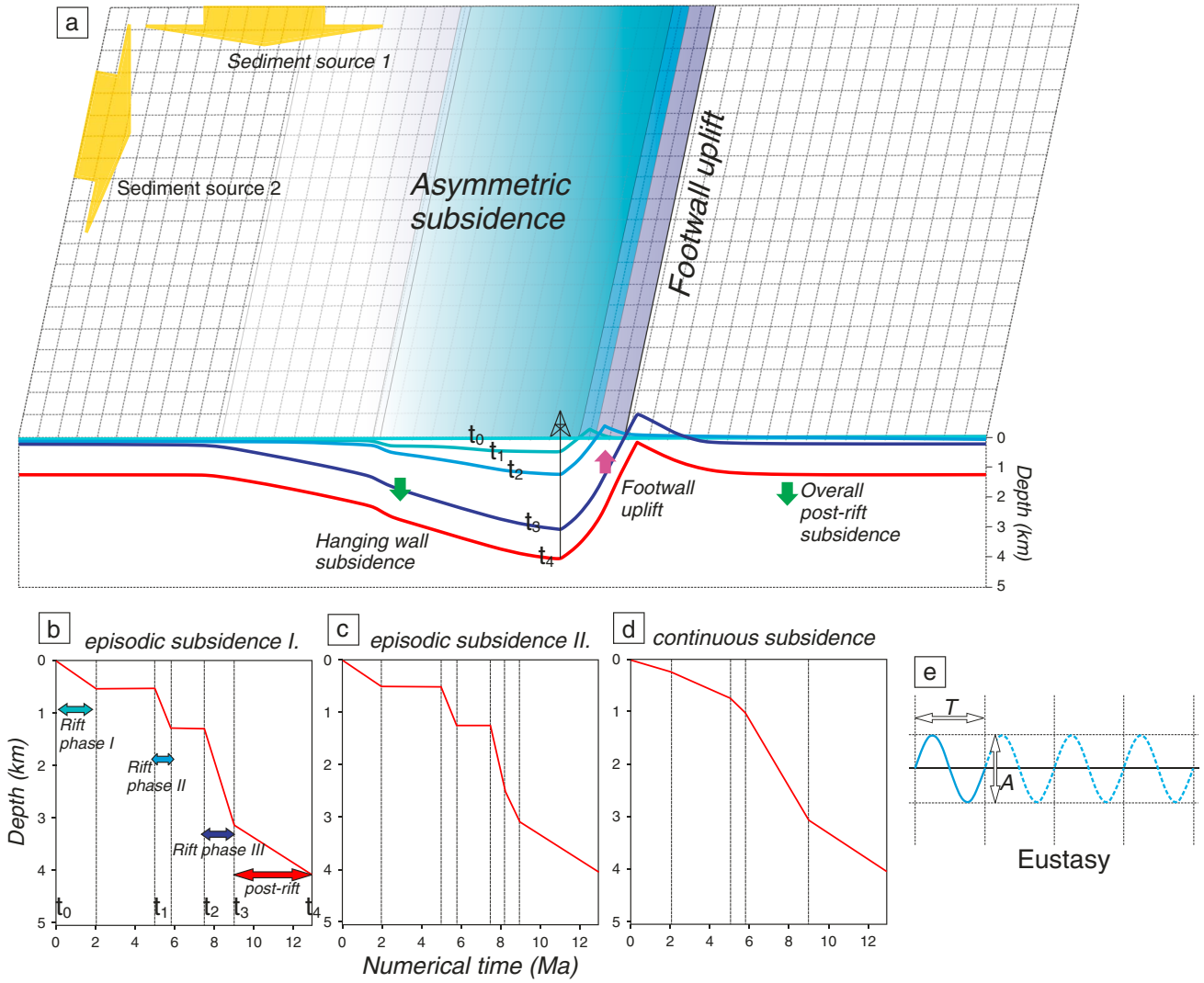

Figure 3. Modeling setup of sediment transport and deposition in half-grabens. (a) Geometry of the numerical model. The first setup assumes 80 × 80 equally spaced cells with 0.5 km equal spacing (i.e., 40 × 40 km modeled area). The second setup assumes 100 × 100 equally spaced cells with 1 km equal spacing (i.e., 100 × 100 km modeled area). Water discharge and sediment flux in the model are defined parallel with and perpendicular to the strike of the half-grabens in their hanging wall close to a corner of the model by a kilometer-scale channel where a linear function of increasing water and sediment amounts to the center of this channel is assumed. The vertical movements recorded by the half-graben and its neighboring area are defined by preimposed basement subsidence maps (t_0–t_4); Illustrative basement subsidence curves for the center of the half-graben in different modeling scenarios assuming episodic scenarios (b) I (reference model) and (c) II and (d) continuous subsidence. (e) Illustration of the assumed eustatic variation that change their time period (*T*) and amplitudes (*A*) in different scenarios.

generic lithology-dependent porosity-burial depth curves (see Figure S1 in the supporting information) taken from borehole measurements from the Pannonian Basin (Szalay, 1982). The calculation dynamic time step is variable from hundreds of years up to 20 kyr. Therefore, the vertical resolution of our numerical model is variable from tens of meters up to hundreds of meters, as a function of sedimentation rate.

We interpret our modeling results by comparing the deposition in the proximal, shallow part of the half-graben overlying the hanging wall flank at far distances from the fault with the sedimentation observed in the deep, main depocenter. Sediments are classified by using a simplified scheme based on the modeled lithology that takes into account the ratio of fine- and coarse-grained rocks, the corresponding paleo-water depth during deposition, and finally, the modeled sedimentary architecture, i.e., horizontal layered, small-scale oblique or clinoform geometries. Based on these attributes, we made a differentiation between small-scale coarse-grained deltas on the shelf, sandy lobes in the basin, footwall derived fans in the

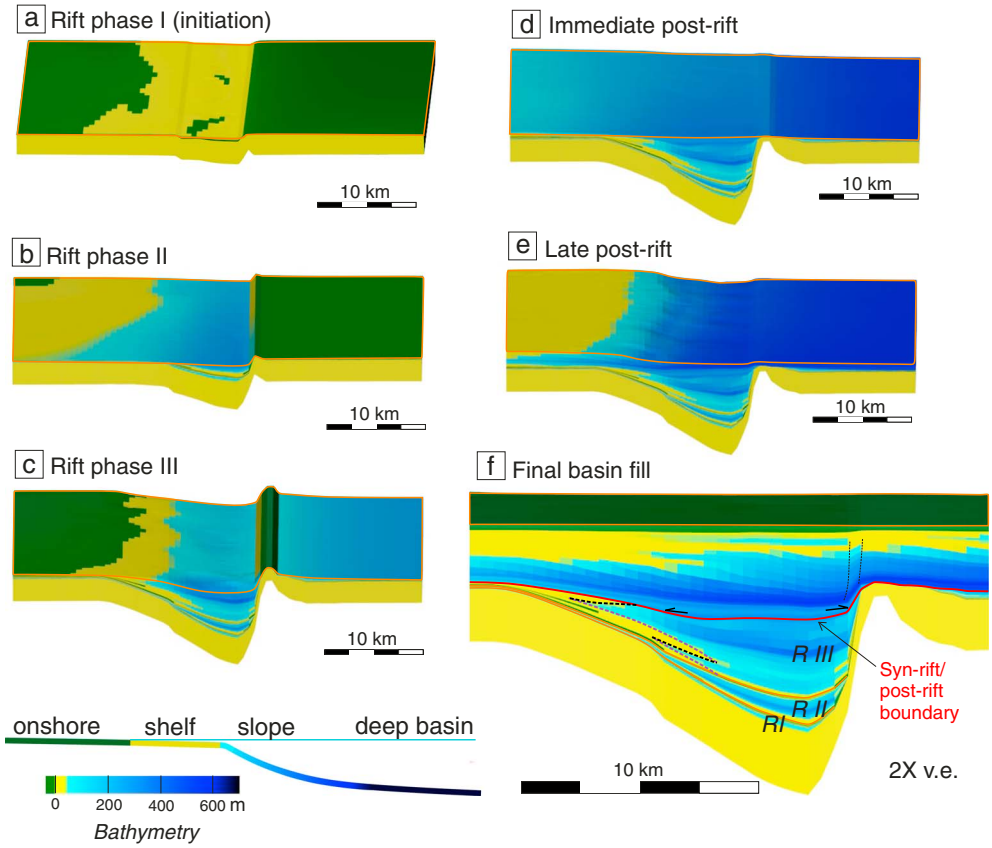

Figure 4. Evolution of bathymetry in the reference experiment at the initial (a) rift phase I, (b) rift phase II, (c) rift phase III, (d) immediate postrift, (e) late postrift, and (f) final basin fill. Note that the final basin fill is shown in a different perspective and scale and zoomed into the half-graben synrift sediments. The red line indicates the synrift/postrift boundary; the orange lines indicate rift phase boundaries. The purple and black dashed lines at the flank of the hanging wall indicate retrograding-prograding high-order cyclicity within the third rift cycle. An episodic basement subsidence was used (Figure 3b) with an eustatic variation period (*T*) of 0.7 Myr and amplitude (*A*) of 70 m, water discharge (*Q*) of 200 m^3/s, short-/long-term discharge ratio (*R*) of 20, and a source mud/sand ratio of 7/3. The three rift phases are reflected by a low-order change in paleobathymetry that is superposed over a higher-order change in paleobathymetry, which is driven by a combination between eustatic cycles and lateral autocyclic sedimentary processes. This cyclicity is well visible in the hanging wall area fed by the sedimentary influx but also in the distal hanging wall area fed by the uplifting and eroding footwall during the rift cycles. This latter source becomes buried during the postrift phase. The orange contour line indicates the top of sediments.

footwall proximity, and large-scale dominantly muddy shelf-margin slope sedimentation connecting the sandy-muddy shelf and the deep basin.

2.2. Model Geometries and Boundary Conditions

An area of 40 × 40 km^2 is modeled in a first series of experiments, where one half-graben is fed by water discharge and sediment influx defined at the boundary and close to the model corner (Figure 3). We defined a reference model (Figures 4 and 5) that is subsequently analyzed by the means of a parametrical study, where the variability of other factors, such as subsidence rates, eustatic water-level variations (Figure 6), and the boundary water discharge (Figure 7), is tested. The tectonic-induced vertical motions of the basement and their evolution through time are preimposed in our models (Figure 3). These were defined based on average observations in natural situations derived from seismic and well data and previous numerical modeling results (Balázs et al., 2017; Ellis et al., 1999; Maniatis et al., 2009). The tectonic elongation during extension are simulated by a preimposed progressively increasing distance between the subsiding depocenter and the uplifting footwall, assuming a fault dip angle of 40° near the surface. Our preimposed tectonic evolution is similar to many natural scenarios, such as half-grabens of the Corinth Rift (Nixon et al., 2016) or the Pannonian Basin (Balázs et al., 2016), where 3–4 km of hanging wall subsidence was associated with kilometer-scale footwall uplift. We note that such geometries approximate the asymmetric extension of intermediate values observed in nature. It is intermediate between a low-offset half-graben and a large-scale

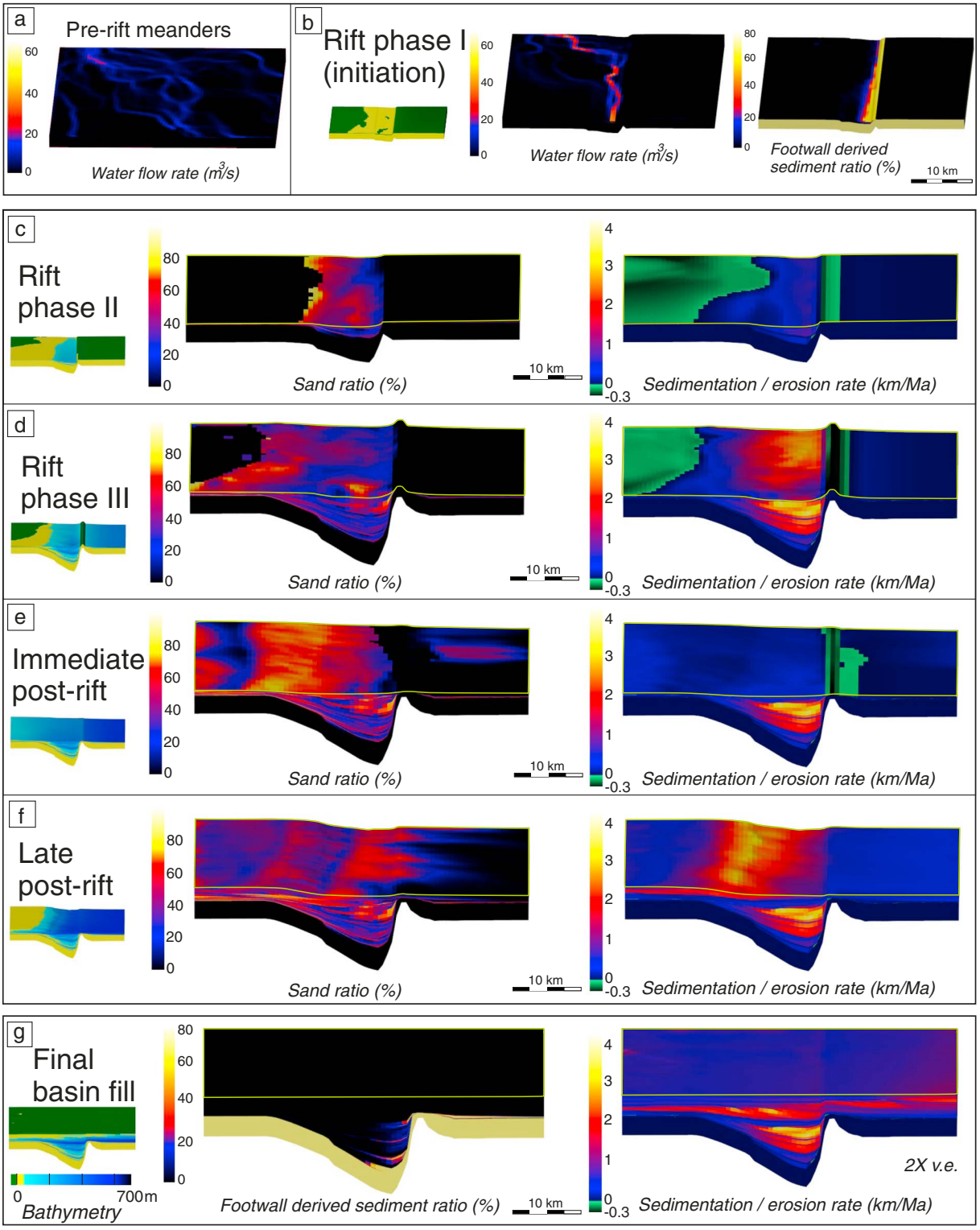

Figure 5. Modeled sediment composition, sedimentation rate, and water flow in the reference experiment. Same parameters are applicable as in Figure 4. (a) The distribution of the water flow rate at the beginning of the model, i.e., after the first time step and before the onset of deformation in the half-graben. (b) Water flow rate and footwall-derived sediment ratio at rift phase I. (c–f) Sedimentary sand ratio and sedimentation or erosion rate for the subsequent rift phase II, rift phase III, immediate postrift, and late postrift periods, respectively. (g) Footwall-derived sediment ratio and sedimentation rate at the end of the model. The light green contour line indicates the top of sediment infill. In our experiments, sediments are defined as a mixture of three grain-size fractions: coarse sand, fine mud, and basement classes. Sand ratio means the proportion of the coarse sand fraction in each voxel. This results in our models in an yellower color indicating coarser sediments; a dark bluer color indicates more fine-grained sediments.

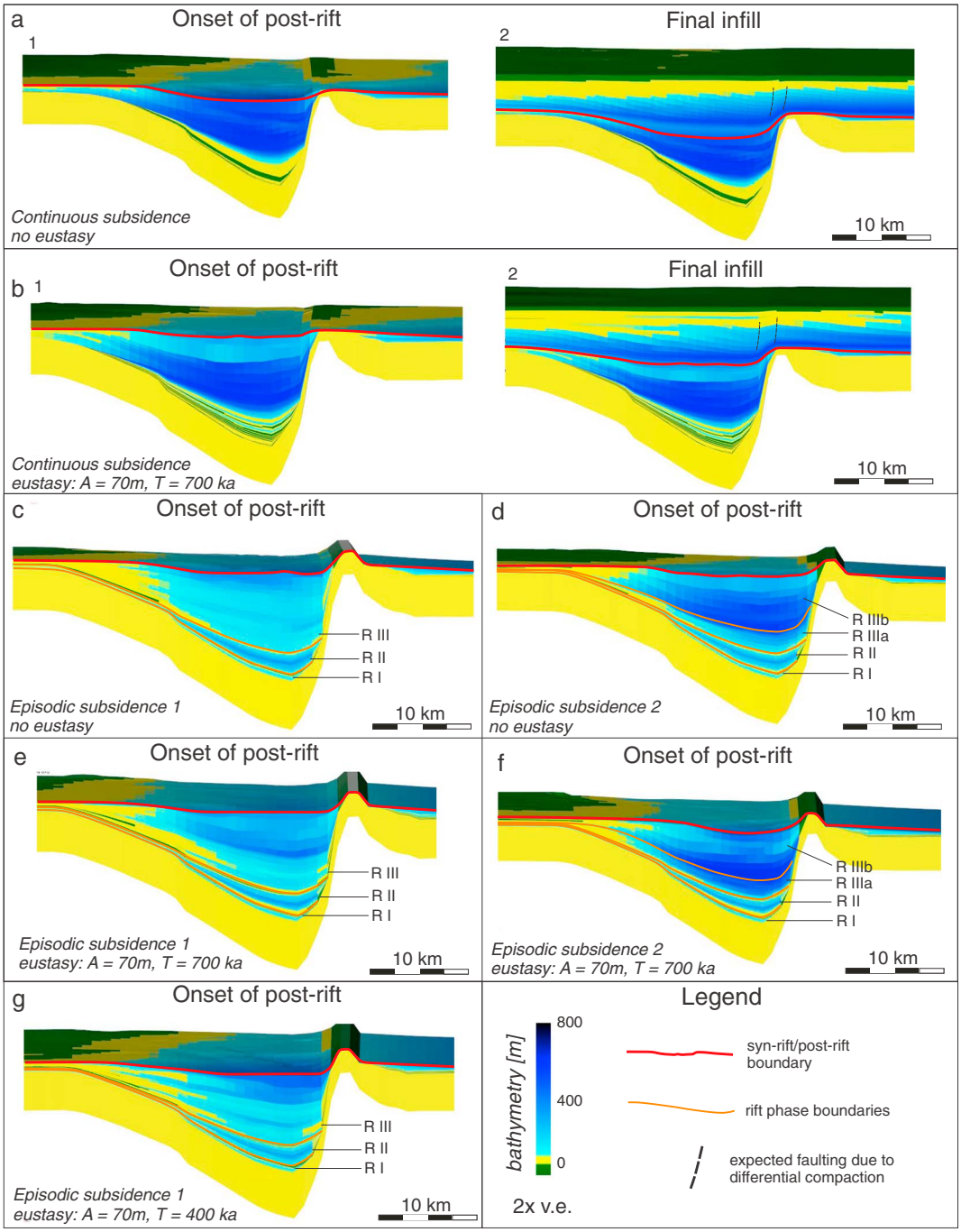

Figure 6. Parameter study analyzing the influence of eustatic variations, their period (*T*), and the influence of the type of basement subsidence (continuous versus variable episodic) on the paleobathymetric evolution of the models. The episodic subsidence scenarios I, episodic subsidence II, and continuous subsidence are illustrated in Figures 3b–3d, respectively. Note the retrograding-prograding pattern of low-order rift cyclicity in experiments with episodic subsidence combined with a higher-order pattern of retrogradation-progradation controlled by a combination of eustatic cycles and lateral autocyclic sedimentary processes.

detachment where normal faults become near horizontal due to progressive tilting, rotations, isostatic response, or rolling hinges (e.g., Angelier & Bergerat, 1983; Buck, 1988; Spencer, 1984; Wernicke, 1985).

Basin formation is initiated by a pair of antithetic normal faults, with different offsets (Figure 3). This initial phase simulates the typical geometry of extensional initiation observed in rift basins (e.g., Prosser, 1993). The larger offset normal fault continues its activity during the later stages of extension. Although the same

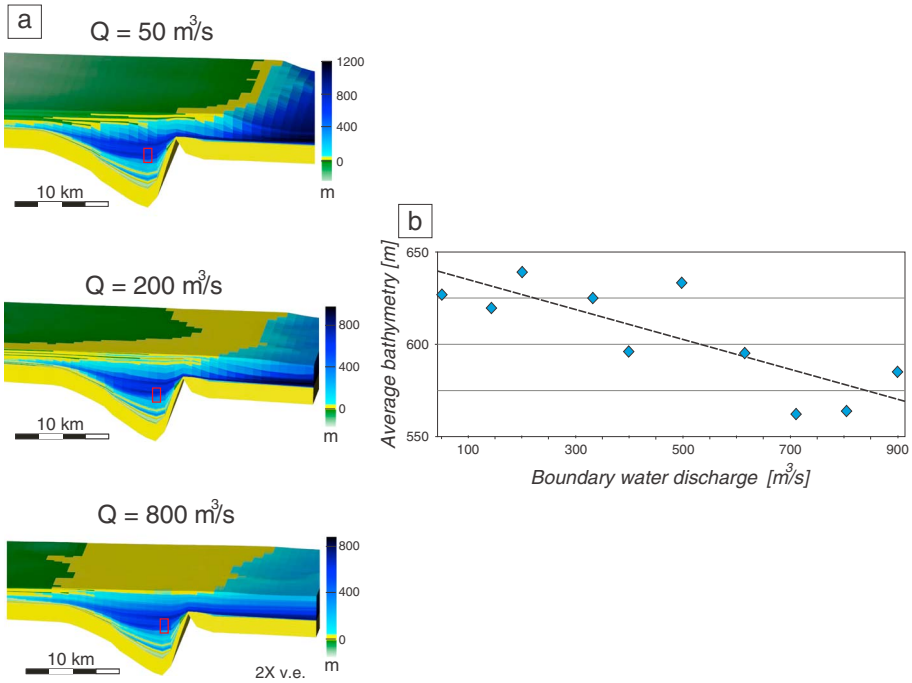

Figure 7. Parameter study analyzing the influence of water discharge (*Q*) into the model. This water discharge is associated with the same amount of sediment influx, but sediments are transported over larger distances at higher discharges. (a) The paleobathymetric evolution of the model. (b) Plot showing the influence of water discharge on the paleobathymetry of a selected time and space interval (red rectangles in Figure 7a) selected near the end of rifting in the depocenter of the basin. Note the main anticorrelation trend, while the variability is controlled by lateral autocyclic sedimentary processes.

amount of total basement subsidence is applied in all models in the center of the half-graben, three different subsidence rate scenarios are compared, which assume continuous or episodic basement subsidence pulses with different subsidence rates at different rifting moments (Figures 3b–3d). The continuous or the episodic basement subsidence pattern defines phases of sedimentation during the synrift evolution that take place in all models for a total of 9 Myr. These can be generally grouped into tectonic system tracts, such as rift initiation, rift climax, and immediate and late postrift periods (cf., Prosser, 1993), although the creation of these tectonic system tracts is not specifically implied. The overall chosen patterns of basement subsidence, characterized by a low rate at the onset of rifting, followed by a subsequent gradual acceleration, are specific to observations in asymmetric extensional systems (e.g., Balázs et al., 2017; Burov & Poliakov, 2003). The synrift phase is followed by 4 Myr of uniform basement subsidence everywhere in the model area (Figures 3b–3d), simulating a postrift thermal sag that takes place at a much larger scale than the one in the half-graben. Different eustatic variation amplitudes and frequencies are simulated to analyze the influence and interactions between tectonic subsidence and sea level variations (Figure 3e). The boundary sediment flux is defined as constant for one synrift phase in such a way that a balance is kept with the rate of creating accommodation space during the same phase. The exception is the last 2 Myr of postrift thermal subsidence, when the sediment supply is significantly increased (doubled when compared with the rate of previous sedimentation). This increase simulates the final stage of a rapid fill in extensional basins, when deltaic influxes from major rivers are often recorded (Sztanó et al., 2013; Matenco et al., 2013). Another important sediment source area is the uplifted and gradually eroding footwall. Water discharge is set between 50 and 900 m^3/s, resembling different climatic conditions. Furthermore, climatic variations are also simulated by the definition of wet short-term and dry long-term intervals (Figure 8). This modeling approach assumes that during each time step ~20% of the sediment influx defined at the boundary of the modeling area is characterized by a higher water discharge value during wet short-term than during dry long-term intervals. This discharge ratio between dry and wet periods is analyzed in the parametric study.

Another series of experiments is applied to a larger area (100×100 km^2) that includes four half-grabens to simulate the synrift subsidence, erosion, and sedimentation of the Great Hungarian Plain of the Pannonian

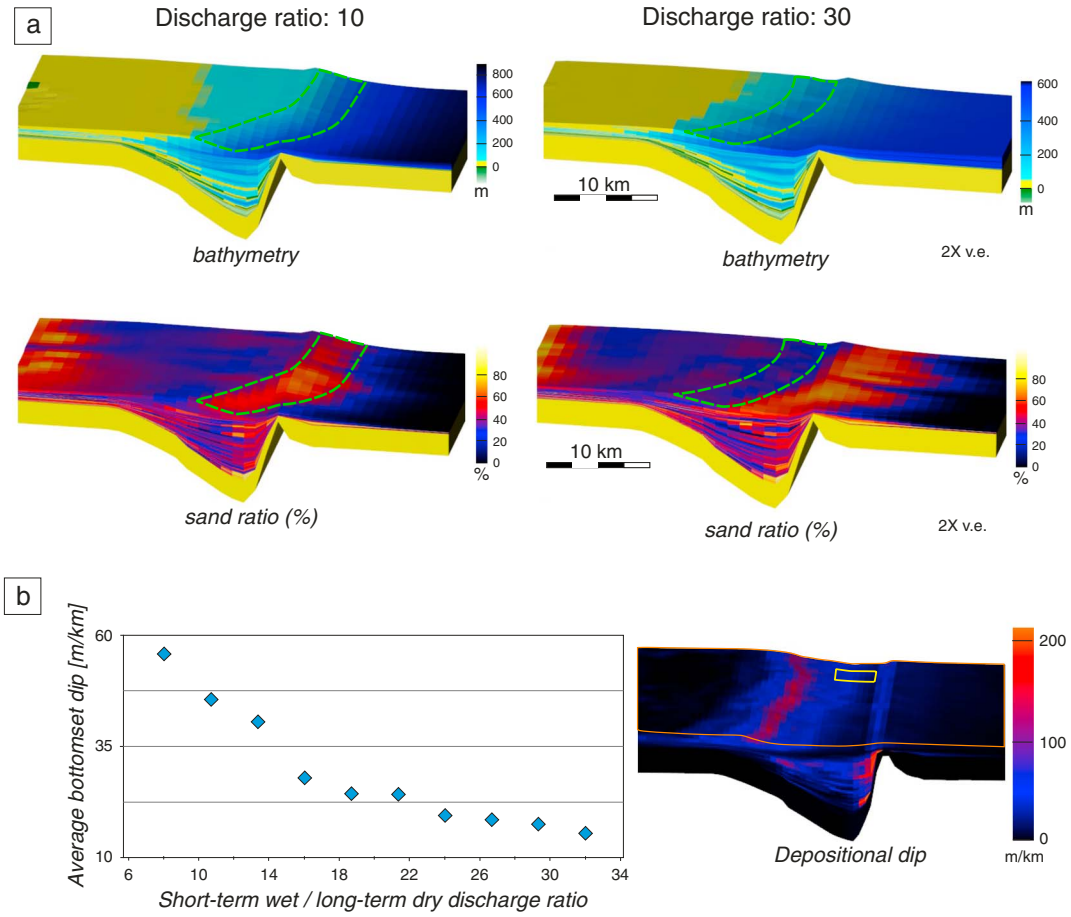

Figure 8. Parameter study analyzing the influence of water discharge ratio (*R*) between wet short-term and dry long-term intervals (see methodology description). (a) Paleobathymetric evolution and sedimentary sand ratio during late postrift progradation. Note that shelf-margin slope (drawn with green dashed line) is steeper and more coarse-grained for lower discharge ratios, while the bottomsets contain a higher proportion of sands at higher discharge ratios. (b) Plot (left) showing the influence of discharge ratios on the average bottomset dip paleobathymetry of a selected time and space interval (yellow rectangle on the right figure). Note the anticorrelation trend. The orange contour line indicates the top of sedimentary infill.

Basin (Figures 9 and 10). Basement subsidence histories derive from available seismic interpretations and backstripped well data (Figure 2, Balázs et al., 2016). Modeling results are presented at four representative moments of basin evolution, showing cross sections through the subbasins at the end of the overall synrift phase at 8.5 Ma. This novel synrift modeling applied to the Pannonian Basin complements and is calibrated by available postrift stratigraphic modeling studies available in the same region, which use the same DionisosFlow modeling software (Csató et al., 2013, 2015).

3. Numerical Modeling of Sedimentation in One Half-Graben

The reference model is designed to simulate an asymmetric and variable basement subsidence in the hanging wall depocenter of one half-graben (Figure 3b), associated with synkinematic and postkinematic sedimentation (Figures 4 and 5). The 9 Myr of synrift evolution is subdivided into multiple synrift phases. The first extensional pulse assumes 2 Myr of moderate basement subsidence rate (~0.25 km/Ma), followed by 3 Myr of zero tectonic subsidence (Figure 3b). In this synrift phase, deposition keeps pace with the tectonically induced basement subsidence (Figure 4a), the accommodation space is filled by alluvial and shallow delta sediments, and footwall-derived fans are deposited in its proximity, while the sediment flux and water flow geometry is conditioned by the opening of the half-graben (Figure 5).

The subsequent 4 Myr contain two rapid pulses of acceleration of the normal fault offset (higher rate of basement subsidence, 0.7 km/Ma) separated by a period of zero subsidence, which simulate a rift climax period

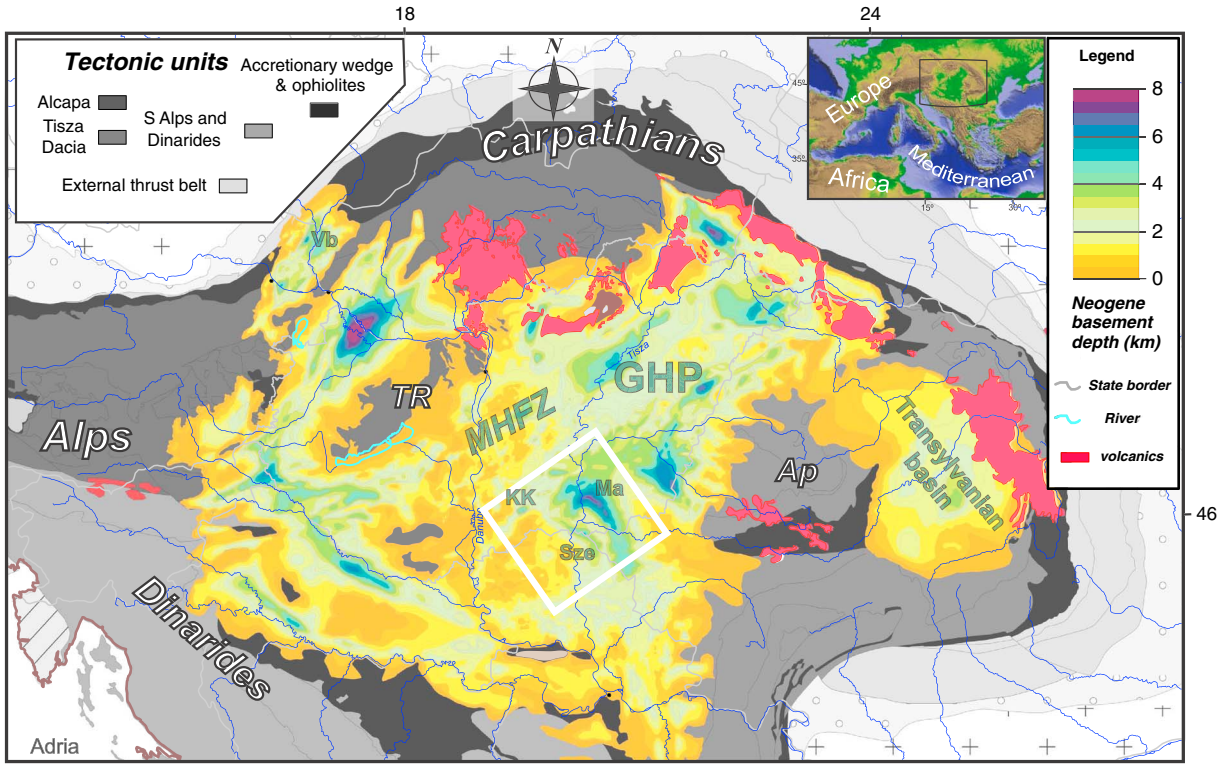

Figure 9. Application of our modeling to the natural case of the Miocene synrift evolution of the SE part of the Great Hungarian Plain of the Pannonian Basin system. The map shows simplified basement tectonic map of the Alps-Carpathians-Dinarides region overlain by the Miocene-Quaternary sedimentary thickness (in kilometers) of the Vienna (Vb), Pannonian, and Transylvanian basins (simplified after Schmid et al., 2008, and Balázs et al., 2017). MHFZ, Mid Hungarian Fault Zone; TR, Trans-Danubian Range; KK, Kiskunhalas subbasin; Ma, Makó Trough; Sze, Szeged Basin.

(t2 and t3 in Figure 3b). The flank of the hanging wall at larger distances from the depocenter is dominated by alluvial and delta environments. The sediments of clastic lobes are sourced from the hanging wall and by footwall erosion and are transferred to the narrow and deep depocenter reaching high sedimentation rates (~3 km/Ma; Figure 5d). In more detail, the second synrift phase results in an overall retrogradation to a maximum water depth of ~200 m, which is subsequently filled by rapid progradation during regression associated with the period of zero subsidence. This evolution is repeated during the third synrift phase, when yet again a rapid retrogradation is recorded to a maximum water depth of ~400 m, followed by progradation (Figure 4c). In this model setup, this progradation is enhanced by this time with a period of sea level fall at the end of this synrift phase. A higher-order retrograding-prograding cyclicity of small-scale delta slopes and lobes is deposited over the hanging wall, controlled by sea level variations and lateral autocyclic processes affecting the sediment flux (Figure 4c). Interestingly, these variations create moments when sand lobes are transported into the deeper parts of basin (Figures 5c and 5d). The rapid uplift of the footwall is only partly accompanied by erosion, which forms a positive topography at the end of the synrift period. This topography prevents bypass and transfer of sediments from the source area over the half-graben and deposition over its footwall (see also Sinclair & Tomasso, 2002). At this time the distal deposition over the footwall is exclusively sourced by its erosion. As the topographic high is progressively eroded, the sediments ultimately bypass and are deposited over the footwall ~2 Myr after the onset of postrift times (during late postrift; Figures 5e and 5f).

The 4 Myr period of postrift thermal subsidence (t_4 in Figures 3a) marks a change from focused subsidence in the depocenter of the half-graben to regional subsidence that creates an overall retrogradation over a marked unconformity at the beginning of postrift times (Figures 4d–4f). This unconformity resembles the geometry of a breakup unconformity, created at the transition between rifting and drifting during the evolution of passive continental margins (e.g., Ziegler & Cloetingh, 2004). During this major retrogradation, deepening of the basin occurs, which results in maximum water depths in the order of 600 m located in the

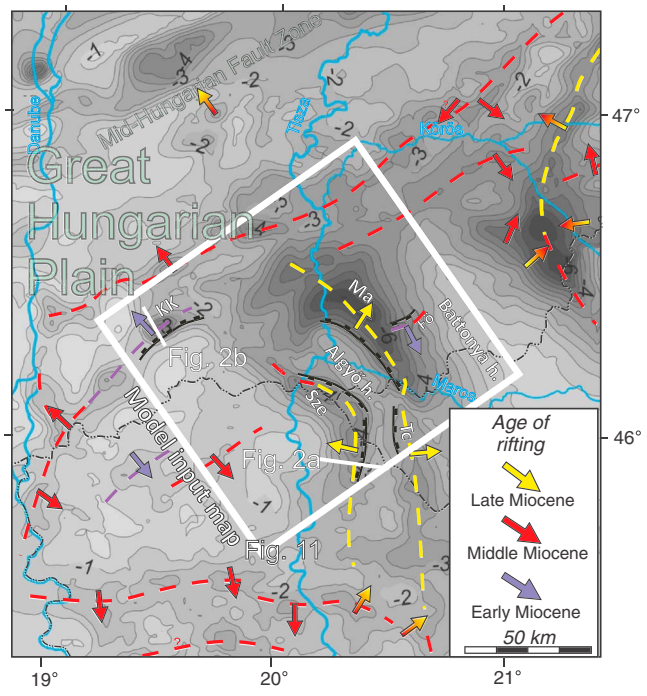

Figure 10. Neogene basement isopach map of the SE part of the Great Hungarian Plain with the location of the main depocenters with their strike (dashed lines), age of rifting, and the main direction of extensional tectonic transport in the various subbasins (the same color-coded arrows (after Balázs et al., 2016)). The white lines show the locations of the interpreted seismic sections. The white square indicates the modeled area of Figure 11. Boundary normal faults of the modeled half-grabens are indicated.

part that overlies the footwall at far distances from the fault (Figure 4d). The erosion of the footwall gradually decreases as it progressively submerges to form later a positive seafloor morphology. This morphology still prevents bypass of coarse-grained sediments. The main sediment flux is transported in the half-graben depocenter, with only thin sand lobes deposited over the distal footwall during wet short-term intervals (Figure 5e). The rapid increase in sediment supply during the last 2 Myr leads to the formation of a large-scale prograding sequence, where deposition of slope sediments connects a deltaic environment with the few hundred meters deep basinal areas (Figures 4e and 4f). The height of this prograding slope is larger over the underlying half-graben depocenter due to differential compaction effects added to the overall basement subsidence. Differential compaction also significantly decreases the overall thickness of the underlying synrift sediments. The interplay between the low postrift basement subsidence rate (~0.22 km/Ma) and sea level variations controls the formation of prograding, aggrading, and/or retrograding clinoform cyclicity (Figure 4f). During these times, sedimentation rate reaches its maximum at the slope, while coarse-grained sediments are partitioned between the shelf and at the toe of slope. Although, there is still minor positive morphology over the eroded footwall, the sediment transport, which takes places by high energy currents, overcomes and the sand lobes can be deposited at much larger distances that can reach ~25 km from the shelf edge (Figure 5f).

3.1. Parameter Sensitivity Analysis

In a series of seven experiments we have analyzed the effects of different basement subsidence scenarios combined with different eustatic frequencies and amplitudes on half-graben synkinematic sedimentation (Figure 6). The first experiment with zero eustatic variations and a continuous basement subsidence pattern (Figure 3d) shows a gradual increase in water depth toward the half-graben depocenter during the synrift phase. The minor variation in the proximity of the footwall is the result of local sourcing due to erosion and redeposition (Figure 6a). In this situation, the late postrift progradation shows a continuous prograding and aggrading pattern. When sea level variations with amplitude of 70 m and period of 700 kyr are added in a second experiment, high-order retrograding-prograding variations are observed during the entire evolution in the shallow part of the basin by moments of progradation, aggradation, and retrogradation, which reflect cycles of transgression, normal and forced regression (Figure 6b). The comparison of these two experiments shows the impact of high-order sea level variations.

The following four experiments follow the same pattern, analyzing the effects of the two types of episodic subsidence (Figures 3b and 3c). When sea level variations are absent, the rift initiation and the subsequent second rift phase show similar retrogradation-progradation cycles (Figures 6c and 6d). Starting from this setup, a small modification in the basement subsidence rate at the end of the third rift phase creates a significant effect (Figures 3b and 3c). In the first scenario (Figure 6c), the rapid basement subsidence during the entire third phase shows a gradual overall retrogradation along the hanging wall followed by the onset of progradation during postrift times. In the second scenario (Figure 6d), the rapid basement subsidence is decreased at the end of the third synrift phase, which creates a retrogradation-progradation pattern (IIIa and IIIb), followed by one other retrogradation-progradation during postrift times. In both scenarios, higher-order retrogradational-progradational cycles visible in the proximal sedimentation of the hanging wall during the third synrift phase reflect lateral autocyclic processes. These autocyclic processes are less visible when sea level variations are present in our models (Figures 6e and 6f), which create a higher-order retrogradation-progradation cyclicity superposed over the lower order one induced by the three rift phases. The fact that this higher-order cyclicity is driven by sea level variations is demonstrated by its dependence on the eustatic frequency, as observed

when this frequency is changed in a subsequent experiment (higher-frequency and higher-order cycles in Figure 6g).

The separation between tectonic and eustatic effects is best observed in our models during the third rift cycle at high sedimentation rates, when the higher-order sea level variations are particularly well visible. Eustatic effects are superimposed on the low-order tectonic variations (Figure 6g, compare with Figures 6e and 6f).

The influence of external water influx value (Q_w) is analyzed in a series of experiments where all other parameters are kept identical with the reference model (Figure 7). In our diffusion modeling approach, this discharge value influences the sediment transport distance, with higher discharge values enabling transportation over larger distances (cf., Gvirtzman et al., 2014). Three models were conducted that simulate relatively low, medium, and high water discharge values (50, 200, and 800 m^3/s, respectively; Figure 7a). This shows that a higher water discharge value creates a wider shallow-water shelf environment, with a lower dip angle of the shelf-margin slope and lower water depth averages in the depocenter. This dependence is best illustrated by the average water depth values of a small volume located in the same area within the deep-water part of the basin (red square in Figure 7a). This shows a clear correlation between decreasing bathymetry with increasing water discharge.

The influence of climate was tested in a series of 10 consecutive models, where the ratio between wet short-term and dry long-term discharge values (R) is changed (Figure 8). At higher ratios, simulating a gradually wetter climate associated with a higher water discharge, sediments will be transported at larger distances, delivering more effectively the sand fraction (Figure 8). At low ratios simulating a balanced, drier climate, most of the sediments remain near the shelf slope (Figure 8a). The influence of climate in building the clinoform geometries was studied by the average dip angle of the bottomsets during the postrift phase. The results show that higher discharge ratios result in more elongated clinoform geometries, characterized by lower dip angles and more coarse-grained bottomsets (Figure 8b).

4. Synrift Sedimentation in the Pannonian Basin System

The variability of the Miocene extension observed in the Great Hungarian Plain of the Pannonian Basin mirrors the evolution of back-arc extension, during the gradual clockwise rotation of the underlying Tisza-Dacia mega-unit, associated with the Carpathian slab retreat and invasion of its external embayment (Figure 9) (see Tari et al., 1999, and Horváth et al., 2015, for further details). The result is a gradual activation and evolution of extensional half-grabens that have different strikes and extensional directions during Miocene times. Therefore, these differently oriented half-grabens show also diachronous synrift sedimentation and transition to the postrift phase (Figure 10) (Balázs et al., 2016). In the Great Hungarian Plain, we have selected a modeling area of 100 × 100 km that includes the evolution of Kiskunhalas, Szeged, Földeák, and the larger Makó half-graben (white rectangle in Figures 9 and 10). The subsidence history of these half-grabens (Figure 2c) and the larger area is constrained by the interpretation of a dense network of seismic and well data (Figures 2a and 2b) (see also Tari et al., 1999; Pigott & Radivojević, 2010; Balázs et al., 2016). The gradual Miocene extensional activation constrains the basement subsidence that has an episodic or continuous pattern for each of these half-grabens (Figure 2c). These half-grabens were filled by sediments sourced dominantly from the neighboring orogens, such as the Dinarides, Alps, and Carpathians by fluvial systems associated, for instance, with the former location of the Danube and Tisza rivers (Magyar et al., 2013).

The modeled retrograding-prograding cyclicity is constrained by recent seismic interpretations analyzing reflection terminations and the overall distribution of seismic facies units (Balázs et al., 2016). These have shown, for instance, that the Kiskunhalas half-graben was controlled by a NNW dipping low-angle normal fault with a highly eroded footwall and was filled with ~3 km lower Miocene synkinematic sediments grouped into four retrograding-prograding cycles (Figure 2b). This middle Miocene immediate postrift is separated by a gently folded erosional unconformity from the overlying late Miocene sediments, created by inversion during latest middle Miocene-earliest late Miocene times. Finally, the Szeged half-graben was controlled by a low-angle normal fault dipping westward with a highly eroded footwall and 2.5 km of middle to early late Miocene synrift and late Miocene-Quaternary postrift sedimentation associated with retrograding-prograding cycles (Figure 2a). All the various half-grabens were subsequently affected by a late postrift subsidence that took place at the much larger scale of the entire Great Hungarian Plain (see further details in Magyar et al., 2013; Sztanó et al., 2013; and Csató et al., 2015).

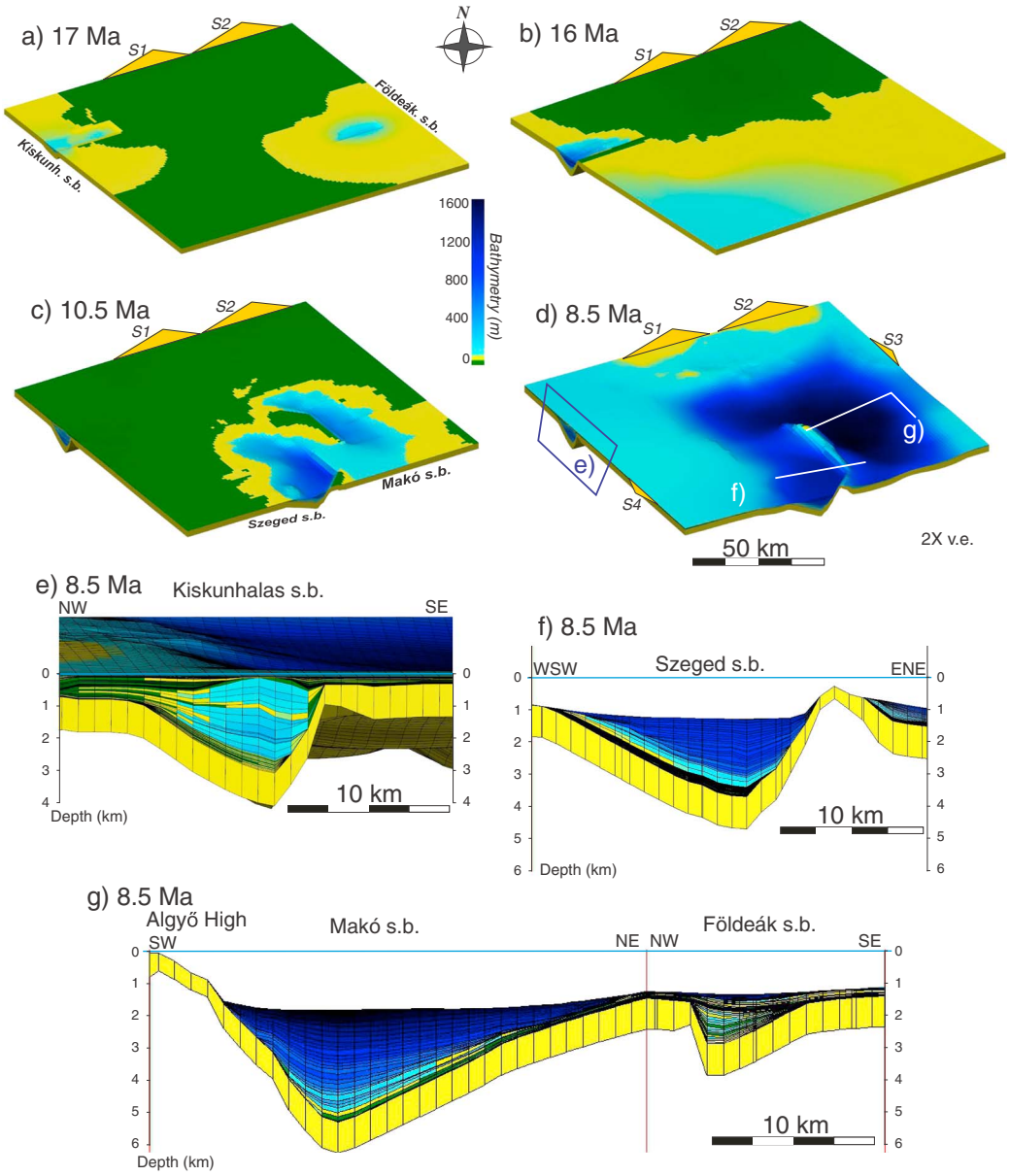

Figure 11. Results of the second modeling setup aimed to simulate the patterns observed in the synrift sedimentation of the Pannonian Basin. The postrift patterns have already been well simulated by similar type of numerical modeling in other studies (Csató et al., 2013, 2015). (a–d) Evolution of bathymetry in the second modeling setup that assumes the gradual fill over multiple half-grabens. The yellow triangles illustrate the influx of water and sediments in the model. Note that the stages are displayed at stratigraphic ages with the onset of the model at 19 Ma; (e–g) comparative modeled cross sections over the four half-grabens displayed at the same stratigraphic time. Location of the cross sections is displayed in Figure 11d. The onset of rifting is diachronous, and the basement subsidence patterns are different in various half-grabens (see text description). Note the inverted geometry of the Kiskunhalas Trough (Figure 11e).

4.1. Numerical Forward Modeling of Synrift Sedimentation in the Great Hungarian Plain

The onset of modeling at 19 Ma (early Miocene) is associated with the start of the basement subsidence in the NE-SW oriented Kiskunhalas and Földeák half-grabens, which subsequently captured most of the sourced sediments (Figure 11a). The smaller Földeák half-graben was filled by the end of the early Miocene by footwall-derived fans and sediments sourced from the north, while the Kiskunhalas half-graben still retained shallow-water sedimentation (Figure 11b). The shallow-water environment was maintained during the middle Miocene, when the Kiskunhalas half-graben was filled by immediate and late postrift sediments. At the same time the onset of extension in the Szeged half-graben was associated with the deposition of a rift

initiation cycle. The inversion observed in the Pannonian Basin at the transition to the late Miocene (cf. Figure 2b; ~12–11 Ma (Horváth, 1995)) resulted most likely in exhumation to continental conditions in most of the modeled area outside the deeper parts of the Szeged half-graben. This short quiescence of extension was followed by the activation of the Makó half-graben and the regional subsidence in the SE associated with a transgression (Figure 11c). Eroded and redeposited sediment remnants of the older Földeák half-graben are overlain by the younger synkinematic deposits of the Makó half-graben. The synrift deposition continued in the Szeged and Makó half-grabens until ~8.5 Ma. The regional subsidence and transgression created water depth values exceeding 1 km in these half-grabens (Figure 11d). The increase of sediment influx sourced by the Alps and Carpathians (Magyar et al., 2013; Sztanó et al., 2013) filled by progradation this high accommodation space during subsequent postrift times.

Three representative cross sections have been extracted from our 3-D evolutionary model to illustrate the sedimentary architecture of the half-grabens at the end of the overall synrift extension in the Great Hungarian Plain (~8.5 Ma; Figures 11e and 11f). In the Kiskunhalas half-graben, the first rift initiation cycle is overlain by shallow-marine sediments. Similar to the reference model (Figure 4c), prograding-retrograding shallow delta cycles are deposited over the hanging wall and are controlled by the pulses of fast subsidence during early Miocene times (Figure 11e, compare with Figure 2b). The inversion and formation of the antiformal geometry followed by the late Miocene transgression create onlaps over its flanks during the increase of water depth. In the Szeged half-graben, the shallow-water middle Miocene rift initiation cycle is overlain by one late Miocene retrogradational-progradational cycle above the separating unconformity (Figure 11f). The subsequent rapid late Miocene subsidence combined with the location of this half-graben at larger distance from the sediment source with intervening trapping basins results in a general transgression to high water depths and distal sedimentation in the depocenter (Figure 11f). Similarly, the rapid late Miocene synrift subsidence of the Makó half-graben outpaces the external sediment influx and the one derived from its eroding footwall (Algyő High), resulting ultimately in high water depth and distal sedimentation (Figure 11g). Similar with observations (Sztanó et al., 2013), the Algyő High and other eroding footwalls are also flooded after ~8 Ma and the local sediment redistribution ceases.

5. Discussion

Our modeling yields novel insights in quantifying the tectonic and climatic controls on sedimentation in asymmetric extensional basins and proposes an evolutionary model for the distribution of fine- and coarse-grained lithologies and sedimentary facies in half-grabens and during the subsequent postrift evolution.

5.1. Three-Dimensional Evolutionary Model and Facies Distribution During Asymmetric Extension

Initiation of asymmetric subsidence in half-grabens drives a reorganization of sedimentary environments (Figures 5a and 5b). Even when high sedimentation rate keeps pace with basement subsidence, sediment routing is concentrated in sourcing hanging wall depocenters, while exhuming footwalls hampers external transport but feeds internally both the hanging wall and the hinterland of the footwall. This rift initiation phase contains the largest volumes of gravity-driven redistributed coarse sediments. Due to the asymmetric geometry of the uplifted footwall, most of the eroded materials is transported towards its hinterland and creates a low-angle pediment surface. Only one third part of the material sourced by the eroding footwall is redistributed into the hanging wall depocenter during these times. This is an effect of the asymmetric geometry of the uplifted footwall that controls the drainage divide position (Figure 12). Controlled by the interplay between sedimentation rate and relative water-level variations, a rapid transition from alluvial to marine environment is recorded. Therefore, the footwall-derived sediments can be transported as fan-deltas as early as the rift-initiation phase, such as is the case of the Middle Miocene Szeged half-graben (Figure 11f).

The subsequent rift phases are primarily controlled by larger fault offsets. Rapid subsidence rates during periods of fault activation result in an overall retrogradation, while periods of tectonic quiescence enable progradation (see also Martins-Neto & Catuneanu, 2010). The flank of depocenters records a higher-order transgressive-regressive cyclicity, which is superimposed on the lower order tectonic activity, both creating retrograding-aggrading-prograding delta slopes. Sand lobes can be transported at larger distances into the half-graben during periods of wet climate (Figures 5 and 8), due to high water discharge values and/or sediment influx (e.g., Gong et al., 2016) and farther progradation of deltas toward the deep basin (e.g., Kim

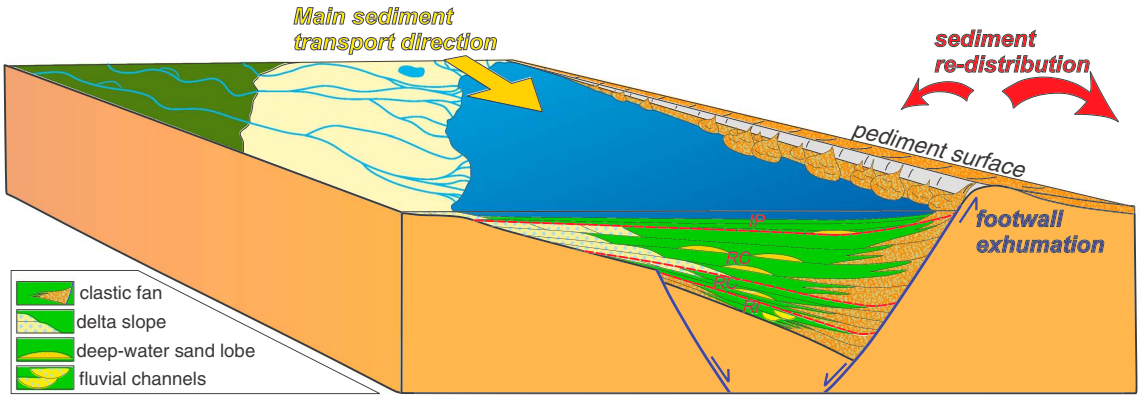

Figure 12. Conceptual model of tectono-sedimentary evolution of a half-graben filled with synkinematic sediments shed from an external hanging wall source and internal footwall erosion displayed at the onset of postrift (IP) time.

et al., 2013). Active fault offsets are associated with moments of footwall uplift and denudation resulting in sediment redistribution towards the depocenters. Erosion rates cannot always keep pace with footwall uplift, and therefore, the deposition of footwall-derived fans may continue during periods of tectonic quiescence as well (Figure 5).

The regional postrift thermal subsidence progressively buries the half-grabens in our models. The footwall of the controlling normal fault may remain above sea level during immediate postrift times and source the depocenter with footwall fans. Subsequently, differential compaction creates gentle syncline geometry above the former hanging wall and induces normal faulting above the footwall (Figures 6 and 2a). Coarse-grained sediments cannot initially bypass the positive morphology of the eroded remnant of the footwall located above or below sea level (Figure 5e). The final bypass and postkinematic fill of half-grabens is only recorded during the late postrift times, when sedimentation rate finally outpaces the thermal subsidence and tectonic controls are minor, when compared to climatic, sea level variations or differential compaction effects. These later effects combined with sediment sourcing influence the sedimentation over the shelf and transport of coarse-grained material toward the deep basin (Figure 5f).

5.2. Tectonic Versus Climatic Controls on Building the Transgressive-Regressive Cyclicity

A robust feature of our numerical modeling of synkinematic sedimentation in asymmetric extension is the evolution of sedimentation cyclicity at different orders (Figures 4 and 6). The retrogradation-progradation pattern observed in our models has obvious coastal onlaps and correlative maximum regression surfaces. Therefore, the conversion to a transgressive-regressive cyclicity is direct (cf. Embry & Johannessen, 1992; Helland-Hansen & Martinsen, 1996). Low-order rift cycles are primarily driven by the variable rates of tectonic-driven subsidence in the half-graben. Moments of active normal faulting result in high subsidence rates and are associated with rapid transgression. The subsequent evolution at lower subsidence rates enables the progressive infill of the created accommodation space, resulting in an overall regression (see also Martins-Neto & Catuneanu, 2010). This means that our rift phases are in fact rift cycles. Such a rift cycle starts with a rapid flooding and an initial retrogradation followed by a prograding and shallowing sequence, which drives an initial fining followed by coarsening upward sedimentary cycle.

Higher-order climatic effects and water-level variations are superimposed on this pattern and can be well observed over the proximal, shallow part of the half-graben. This separation is possible because the rates of the spatially asymmetric tectonic subsidence over the proximal part are much lower when compared to the main depocenter (0.6 km/Myr and 1.8 km/Myr, respectively; Figure 1a). Therefore, the shallower deltaic higher-order transgressive-regressive cycles are better visible over the proximal part. Our models are able to separate autocyclic processes from sea level variations and tectonically induced cycles (cf. Figures 6c, 6e, and 6g) by their amplitude, time period, and correlation with the source area. This separation can be misleading by analyzing onlaps on 2-D sections only and therefore requires 3-D approach to be able to record autocyclic processes acting on different scales from cut-and-fill of channels, avulsions of river and delta channels, and related lobe switching. In the source area, the autocyclic onlaps are directly correlated with the

lateral migration of the river and delta system. This becomes clearer when the accommodation space is larger, such as during our third rift phase that is characterized by a constant, high-rate of basement subsidence creating a retrogradation of the delta environment by ~20 km landward, which is superimposed by higher-order eustatic retrogradation-progradation cycles (Figure 6e). Slight variations in the subsidence pattern may significantly modify the low-order tectonically driven cycles, such as during the third synrift phase, when a minor decrease in subsidence creates an additional retrograding-prograding cycle (compare Figures 6e and 6f). The modeling also shows that lateral autocyclic sourcing variations of the feeding delta create even higher-order cycles both by proximal sedimentation over the flank (Figure 6c) and by deposition of sand lobes in the deep basin (Figure 5). Obviously, such a discrimination of external and internal driving factors in sedimentation depends on the chosen sediment influx, the frequencies and amplitudes of sea level and tectonic variations, and the resolution of our model. For instance, our modeling can simulate the observations at high sediment flux in the Kiskunhalas half-graben of the Pannonian Basin (Figures 2b and 11e), while the low sediment flux and high subsidence rates of the Makó half-graben situated at larger distances from the source area with intervening trapping basins (cf. Sztanó et al., 2013) create distal sediments whose cyclicity is below the resolution of most seismic observations and numerical models (Figure 11g).

6. Conclusions

By conducting a series of 3-D numerical modeling experiments, we have contributed to the understanding of sedimentary infill of asymmetric extension in half-grabens controlled by one major listric normal fault or detachment that drives the sedimentation in hanging walls and the uplift of their footwalls. Observations in key basins, such as the Pannonian backarc of central Europe, show that the asymmetric nature of extension drives a specific deformational pattern: footwall exhumation is associated with moments of low subsidence followed by its acceleration in the center of the half-graben, which are followed by a slower regional thermal subsidence phase. Our modeling shows that such scenarios are associated with continental alluvial to shallow-water sedimentation during the early stages of the synrift, followed by rapid deepening during the subsequent synrift evolution.

Our modeling demonstrates that forcing factors, such as tectonics, sea level variations, or climate, associated with water and sediment influx, have primary control on the sedimentary architecture and control the variability of erosion and lithologies inside the half-grabens and neighboring areas. Our modeling shows the ability to discriminate between the low-order tectonic and higher-order sea level and climatic-driven transgressive-regressive cycles from the autocyclic nature of the depositional system during multiple stages of the synrift and postrift evolution. Unconformities separate these various temporal and spatial orders of the modeled and observed cyclicity. The actual sedimentation rate is linked to tectonics and to climatic variations controlling the distance and transport processes between the sources and the depocenter. A high sediment influx and water discharge during wet climate transport sand lobes at large distances in the deep part of the basin, assisted or not by moments of sea level drop. The depocenter of such extensional structures records large water depth variations, episodic activity of normal faults, and their migration in time, while the flanks record the various orders of transgressive-regressive cyclicity.

We have also modeled a system of multiple half-grabens that are activated in different locations, at different times, and with different kinematics, such as observed in the Great Hungarian Plain of the Pannonian Basin. Modeling demonstrates the complex interplay between direct sediment sourcing and the ability of sediments to bypass trapping basins, compaction-induced geometries, and paleo-reliefs created by eroded footwall geometries. Such obstacles in the pathway of the sediment flux create a distal, often pelagic sedimentation, where our ability to detect moments of activation of various forcing parameters is rather reduced at the standard seismic or wells observational scale.

Acknowledgments

This study was financed by the Netherlands Center for Integrated Solid Earth Science (ISES). Paolo Ballato, an anonymous reviewer, and the Associate Editor Luc Lavier are acknowledged for providing valuable critical reviews that have significantly improved the manuscript. Fruitful discussions and cooperation with Frank Horváth, Imre Magyar, and László Fodor on the evolution of the Pannonian Basin are gratefully acknowledged. Supporting data are available in the supporting information file. The commercial numerical code used in this study can be requested by contacting Beicip-Franlab (www.beicip.com). We thank Beicip-Franlab for providing an academic license for DionisosFlow and CougarFlow.

References

Andrić, N., Sant, K., Matenco, L., Mandic, O., Tomljenović, B., Pavelić, D., … Ooms, J. (2017). The link between tectonics and sedimentation in asymmetric extensional basins: Inferences from the study of the Sarajevo-Zenica Basin. *Marine and Petroleum Geology*, *83*, 305–322.

Angelier, J., & Bergerat, F. (1983). Systèmes de contrainte et extension intracontinentale. *Bulletin des Centres de Recherches Exploration-Production Elf-Aquitaine*, *7*, 137–147.

Balázs, A., Burov, E., Matenco, L., Vogt, K., Francois, T., & Cloetingh, S. (2017). Symmetry during the syn- and post-rift evolution of extensional back-arc basins: The role of inherited orogenic structures. *Earth and Planetary Science Letters*, *462*, 86–98.

Balázs, A., Matenco, L., Magyar, I., Horváth, F., & Cloetingh, S. (2016). The link between tectonics and sedimentation in back-arc basins: New genetic constraints from the analysis of the Pannonian Basin. *Tectonics*, *35*, 1526–1559. https://doi.org/10.1002/2015TC004109

Báldi, K., Benkovics, L., & Sztanó, O. (2002). Badenian (Middle Miocene) basin development in SW Hungary: Subsidence history based on quantitative paleobathymetry of foraminifera. *International Journal of Earth Sciences*, *91*, 490–504.

Baur, J., Sutherland, R., & Stern, T. (2014). Anomalous passive subsidence of deep-water sedimentary basins: A prearc basin example, Southern New Caledonia trough and Taranaki Basin, New Zealand. *Basin Research*, *26*, 242–268.

Bialas, R. W., & Buck, W. R. (2009). How sediment promotes narrow rifting: Application to the Gulf of California. *Tectonics*, *28*, TC4014. https://doi.org/10.1029/2008TC002394

Buck, W. R. (1988). Flexural rotation of normal faults. *Tectonics*, *5*, 959–973.

Burgess, P. M., Lammers, H., Van Oosterhout, C., & Granjeon, D. (2006). Multivariate sequence stratigraphy: Tackling complexity and uncertainty with stratigraphic forward modeling, multiple scenarios and conditional frequency maps. *AAPG Bulletin*, *90*, 1883–1901.

Burov, E., & Poliakov, A. (2003). Erosional forcing of basin dynamics: New aspects of syn- and post-rift evolution. *Geological Society Special Publication London*, *212*, 209–223.

Carson, M. A., & Kirkby, M. J. (1972). *Hillslope form and process* (pp. 475). Cambridge: Cambridge University Press.

Clevis, Q., De Boer, P. L., & Nijman, W. (2004). Differentiating the effect of episodic tectonism and eustatic sea-level fluctuations in foreland basins filled by alluvial fans and axial deltaic systems: Insights from a three-dimensional stratigraphic forward model. *Sedimentology*, *51*, 809–835. https://doi.org/10.1111/j.1365-3091.2004.00652.x

Cloetingh, S., Burov, E., Matenco, L., Beekman, F., Roure, F., & Ziegler, P. A. (2013). The Moho in extensional tectonic settings: Insights from thermo-mechanical models. *Tectonophysics*, *609*, 558–604.

Cloetingh, S., & Haq, B. U. (2015). Inherited landscapes and sea level change. *Science*, *347*(6220), 1258375. https://doi.org/10.1126/science.1258375

Contreras, J., Scholz, C. H., & King, G. C. P. (1997). A model of rift basin evolution constrained by first-order stratigraphic observations. *Journal of Geophysical Research*, *102*, 7673–7690.

Coulthard, T. J. (2001). Landscape evolution models: A software review. *Hydrological Processes*, *15*, 165–173.

Csató, I., Granjeon, D., Catuneanu, O., & Baum, G. R. (2013). A three-dimensional stratigraphicmodel for the Messinian crisis in the Pannonian Basin, eastern Hungary. *Basin Research*, *25*, 121–148.

Csató, I., Toth, S., Catuneanu, O., & Granjeon, D. (2015). A sequence stratigraphic model for the Upper Miocene-Pliocene basin fill of the Pannonian Basin, eastern Hungary. *Marine and Petroleum Geology*, *66*, 117–134.

Culling, W. (1960). Analytical theory of erosion. *Journal of Geology*, *68*, 366–344.

de Leeuw, J., Eggenhuisen, J. T., & Cartigny, M. J. B. (2016). Morphodynamics of submarine channel inception revealed by new experimental approach. *Nature Communications*, *7*, 10886. https://doi.org/10.1038/ncomms10886

Ellis, G. A., Densmore, A. L., & Anderson, R. S. (1999). Development of mountainous topography in the Basin Ranges, USA. *Basin Research*, *11*, 21–41.

Embry, A. F., & Johannessen, E. (1992). T-R sequence stratigraphy, facies analysis and reservoir distribution in the uppermost Triassic-Lower Jurassic succession, Western Sverdrup Basin, Arctic Canada. In T. Vorren (Ed.), *Arctic geology and petroleum potential* (Vol. 2, pp. 121–146). Amsterdam: Norwegian Petroleum Society Special Publication.

Faccenna, C., Becker, T. W., Auer, L., Billi, A., Boschi, L., Brun, J. P., … Jolivet, L. (2014). Mantle dynamics in the Mediterranean. *Reviews of Geophysics*, *52*, 283–332. https://doi.org/10.1002/2013RG000444

Gervais, V., & Masson, R. (2004). Mathematical and numerical analysis of a stratigraphic model. *M2AN*, *38*, 585–611.

Gong, C., Steel, R., Wang, Y., Lin, C., & Olariu, C. (2016). Shelf-margin architecture variability and its role in sediment-budget partitioning into deep-water areas. *Earth-Science Reviews*, *154*, 72–101.

Granjeon, D. (1997). Modélisation stratigraphique déterministe: conception et applications d'un modele diffusif 3D multilithologique, Thèse de Doctorat, Université de Rennes 1.

Granjeon, D. (2014). 3D forward modeling of the impact of sediment transport and base level cycles on continental margins and incised valleys. *International Association of Sedimentologists. Special Publication*, *46*, 453–472.

Granjeon, D., & Joseph, P. (1999). Concepts and applications of a 3-D multiple lithology, diffusive model in stratigraphic modeling. In J. W. Harbaugh, et al. (Eds.), *Numerical experiments in stratigraphy: Recent advances in stratigraphic and sedimentologic computer simulations* (Vol. 62, pp. 197–210). Tulsa, OK: Society for Sedimentary Geology.

Griffiths, C. M., Dyt, C., Paraschivoiu, E., & Liu, K. (2001). Sedsim in hydrocarbon exploration. In D. Merriam & J. C. Davis (Eds.), *Geologic modeling and simulation* (pp. 71–97). New York: Kluwer Academic.

Gupta, S., Cowie, P. A., Dawers, N. H., & Underhill, J. R. (1998). A mechanism to explain rift-basin subsidence and stratigraphic patterns through fault array evolution. *Geology*, *26*, 595–598.

Gvirtzman, Z., Csató, I., & Granjeon, D. (2014). Constraining sediment transport to deep marine basins through submarine channels: The Levant margin in the Late Cenozoic. *Marine Geology*, *347*, 12–26.

Helland-Hansen, W., & Martinsen, O. J. (1996). Shoreline trajectories and sequences: Description of variable depositional-dip scenarios. *Journal of Sedimentary Research*, *66*, 670–688.

Horváth, F. (1995). Phases of compression during the evolution of the Pannonian basin and its bearing on hydrocarbon exploration. *Marine and Petroleum Geology*, *12*, 837–844.

Horváth, F., Musitz, B., Balázs, A., Végh, A., Uhrin, A., Nádor, A., … Wórum, G. (2015). Evolution of the Pannonian basin and its geothermal resources. *Geothermics*, *53*, 328–352.

Horváth, F., Szalay, Á., & Royden, L. H. (1988). Subsidence, thermal, and maturation history of the Great Hungarian Plain. In L. H. Royden & F. Horvath (Eds.), *A Study in Basin Evolution*, AAPG Mem. (pp. 355–372). Tulsa, OK: AAPG.

Karátson, D., Németh, K., Székely, B., Ruszkiczay-Rudiger, Z., & Pécskay, Z. (2006). Incision of a river curvature due to exhumed Miocene volcanic landforms: Danube Bend, Hungary. *International Journal of Earth Sciences*, *95*, 929–944.

Kim, Y., Kim, W., Cheong, D., Muto, T., & Pyles, D. R. (2013). Piping coarse-grained sediment to a deep water fan through a shelf-edge delta bypass channel: Tank experiments. *Journal of Geophysical Research: Earth Surface*, *118*, 2279–2291. https://doi.org/10.1002/2013JF002813

Leeder, M., Harris, T., & Kirkby, M. (1998). Sediment supply and climate change: implications for basin stratigraphy. *Basin Research*, *10*, 7–18.

Magyar, I., Radivojevic, D., Sztanó, O., Synak, R., Ujszászi, K., & Pócsik, M. (2013). Progradation of the paleo-Danube shelf margin across the Pannonian Basin during the Late Miocene and Early Pliocene. *Global and Planetary Change*, *103*, 168–173.

Maniatis, G., Kurfeß, D., Hampel, A., & Heidbach, O. (2009). Slip acceleration on normal faults due to erosion and sedimentation—Results from a new three-dimensional numerical model coupling tectonics and landscape evolution. *Earth and Planetary Science Letters*, *284*, 570–582.

Martins-Neto, M. A., & Catuneanu, O. (2010). Rift sequence stratigraphy. *Marine and Petroleum Geology*, *27*, 247–253.
Matenco, L., Andriessen, P., & the SourceSink Network (2013). Quantifying the mass transfer from mountain ranges to deposition in sedimentary basins: Source to sink studies in the Danube Basin–Black Sea system. *Global and Planetary Change*, *103*, 1–18.
Matenco, L., Munteanu, I., ter Borgh, M., Stanica, A., Tilita, M., Lericolais, G., … Oaie, G. (2016). The interplay between tectonics, sediment dynamics and gateways evolution in the Danube system from the Pannonian Basin to the western Black Sea. *Science of the Total Environment*, *543*, 807–827. https://doi.org/10.1016/j.scitotenv.2015.10.081
Murray, A. B., & Paola, C. (1994). A cellular model of braided rivers. *Nature*, *371*, 54–57.
Nixon, C. W., McNeill, L. C., Bull, J. M., Bell, R. E., Gawthorpe, R. L., Timothy, J., … Kranis, H. (2016). Rapid spatiotemporal variations in rift structure during development of the Corinth Rift, central Greece. *Tectonics*, *35*, 1225–1248. https://doi.org/10.1002/2015TC004026
Olive, J.-A., Behn, M. D., & Malatesta, L. C. (2014). Modes of extensional faulting controlled by surface processes. *Geophysical Research Letters*, *41*, 6725–6733. https://doi.org/10.1002/2014GL061507
Pigott, J., & Radivojević, D. (2010). Seismic stratigraphy based chronostratigraphy (SSBC) of the Serbian Banat region of the Pannonian Basin. *Center European Journal of Geography*, *2*, 481–500. https://doi.org/10.2478/v10085-010-0027-2
Postma, G., Kleinhans, M. G., Meijer, P. T., & Eggenhuisen, J. T. (2008). Sediment transport in analogue flume models compared with real-world sedimentary systems: A new look at scaling evolution of sedimentary systems in a flume. *Sedimentology*, *55*, 1541–1557.
Prosser, S. (1993). Rift related depositional system and their seismic expression. In D. Williams & A. Dobb (Eds.), *Tectonics and Seismic Sequence Stratigraphy* (Vol. 71, pp. 35–66). Geological Society Special Publications. https://doi.org/10.1144/GSL.SP.1993.071.01.03
Schlager, W. (1993). Accommodation and supply—A dual control on stratigraphic sequences. *Sedimentary Geology*, *86*, 111–136.
Schmid, S. M., Bernoulli, D., Fugenschuh, B., Matenco, L., Schefer, S., Schuster, R., … Ustaszewski, K. (2008). The Alpine–Carpathian–Dinaridic orogenic system: Correlation and evolution of tectonic units. *Swiss Journal of Geosciences*, *101*, 139–183.
Sinclair, H. D., & Tomasso, M. (2002). Depositional evolution of confined turbidite basins. *Journal of Sedimentary Research*, *72*, 451–456.
Spencer, J. E. (1984). Role of tectonic denudation in warping and uplift of low-angle normal faults. *Geology*, *12*, 95–98.
Szalay, Á. (1982). *A rekonstrukciós szemléletű földtani kutatás lehetőségei a szénhidrogénperspektívák előrejelzésében* (pp. 146). Budapest: Kandidátusi dolgozat, Hungarian Academy of Sciences. (in Hungarian)
Sztanó, O., Szafián, P., Magyar, I., Horányi, A., Bada, G., Hughes, D. W., … Wallis, R. J. (2013). Aggradation and progradation controlled clinothems and deep-water sand delivery model in the Neogene Lake Pannon, Makó Trough, Pannonian Basin, SE Hungary. *Global and Planetary Change*, *103*, 149–167.
Tari, G., Dovenyi, P., Dunkl, I., Horvath, F., Lenkey, L., Ștefănescu, M., … Toth, T. (1999). Lithospheric structure of the Pannonian basin derived from seismic, gravity and geothermal data. In B. Durand, L. Jolivet, F. Horvath, & M. Serrane (Eds.), *The Mediterranean Basins: Extension within the Alpine orogen* (Vol. 156, pp. 215–250). Geological Society London, Special Publications.
Ter Voorde, M., Ravnas, R., Faerseth, R., & Cloetingh, S. (1997). Tectonic modeling of the Middle Jurassic synrift stratigraphy in the Oseberg–Brage area, northern Viking Graben. *Basin Research*, *9*, 133–150.
Tirel, C., Brun, J. P., & Burov, E. (2008). Dynamics and structural development of metamorphic core complexes. *Journal of Geophysical Research*, *113*, B04403. https://doi.org/10.1029/2005JB003694
Tucker, G. E., & Hancock, G. R. (2010). Modelling landscape evolution. *Earth Surface Processes and Landforms*, *35*, 28–50.
Tucker, G. E., & Slingerland, R. (1994). Erosional dynamics, flexural isostasy and long-lived escarpments: A numerical modeling study. *Journal of Geophysical Research*, *10*(12), 229–243.
van Dijk, M., Postma, G., & Kleinhans, M. G. (2009). Autocyclic behaviour of fan deltas: An analogue experimental study. *Sedimentology*, *56*, 1569–1589. https://doi.org/10.1111/j.1365-3091.2008.01047.x
van Wijk, J. W., & Cloetingh, S. A. P. L. (2002). Basin migration caused by slow lithospheric extension. *Earth and Planetary Science Letters*, *198*, 275–288.
Wernicke, B. (1985). Uniform-sense normal simple shear of the continental lithosphere. *Canadian Journal of Earth Sciences*, *22*, 108–126.
Wernicke, B. (1992). Cenozoic extensional tectonics of the U.S. Cordillera. In B. C. B, P. W. Lipman & M. L. Zoback (Eds.), *The Cordilleran orogen: Conterminous U.S* (pp. 553–581). Boulder, CO: Geological Society of America.
Ziegler, P. A., & Cloetingh, S. (2004). Dynamic processes controlling evolution of rifted basins. *Earth-Science Reviews*, *64*, 1–50.